Supplement of Nat. Hazards Earth Syst. Sci., 18, 1867–1890, 2018
https://doi.org/10.5194/nhess-18-1867-2018-supplement

Natural Hazards and Earth System Sciences
Open Access
EGU

Supplement of

Formation, breaching and flood consequences of a landslide dam near Bujumbura, Burundi

Léonidas Nibigira et al.

Correspondence to: Léonidas Nibigira (leonidas.nibigira@doct.ulg.ac.be)

Table S1. Extended Udden-Wentworth grain-size scale for sedimentary particles, after Blair and McPherson (1999).

(Source : Terry and Goff, 2014).

PARTICLE LENGTH (dI) km	m	mm	Φ	GRADE	CLASS	FRACTION Unlithified	FRACTION Lithified
1075			-30	very coarse	Megalith	Megagravel	Mega-Conglomerate
538			-29	coarse			
269			-28	medium			
134			-27	fine			
67.2			-26	very fine			
33.6			-25	very coarse	Monolith		
16.8			-24	coarse			
8.4			-23	medium			
4.2			-22	fine			
2.1			-21	very fine			
1.0	1048.6		-20	very coarse	Slab		
0.5	524.3		-19	coarse			
0.26	262.1		-18	medium			
	131.1		-17	fine			
	65.5		-16	very coarse	Block		
	32.8		-15	coarse			
	16.4		-14	medium			
	8.2		-13	fine			
	4.1	4096	-12	very coarse	Boulder		
	2.0	2048	-11	coarse			
	1.0	1024	-10	medium			
	0.5	512	-9	fine			
	0.25	256	-8	coarse	Cobble	Gravel	Conglomerate
		128	-7	fine			
		64	-6	very coarse	Pebble		
		32	-5	coarse			
		16	-4	medium			
		8	-3	fine			
		4	-2		Granule		
		2	-1	very coarse	Sand	Sand	Sandstone
		1	0	coarse			
		0.50	1	medium			
		0.25	2	fine			
		0.125	3	very fine			
		0.063	4	coarse	Silt	Mud	Mudstone or Shale
		0.031	5	medium			
		0.015	6	fine			
		0.008	7	very fine			
		0.004	8		Clay		
		0.002	9				
		0.001	10				
		0.0005	11				
		0.0002	12				
		0.0001	13				

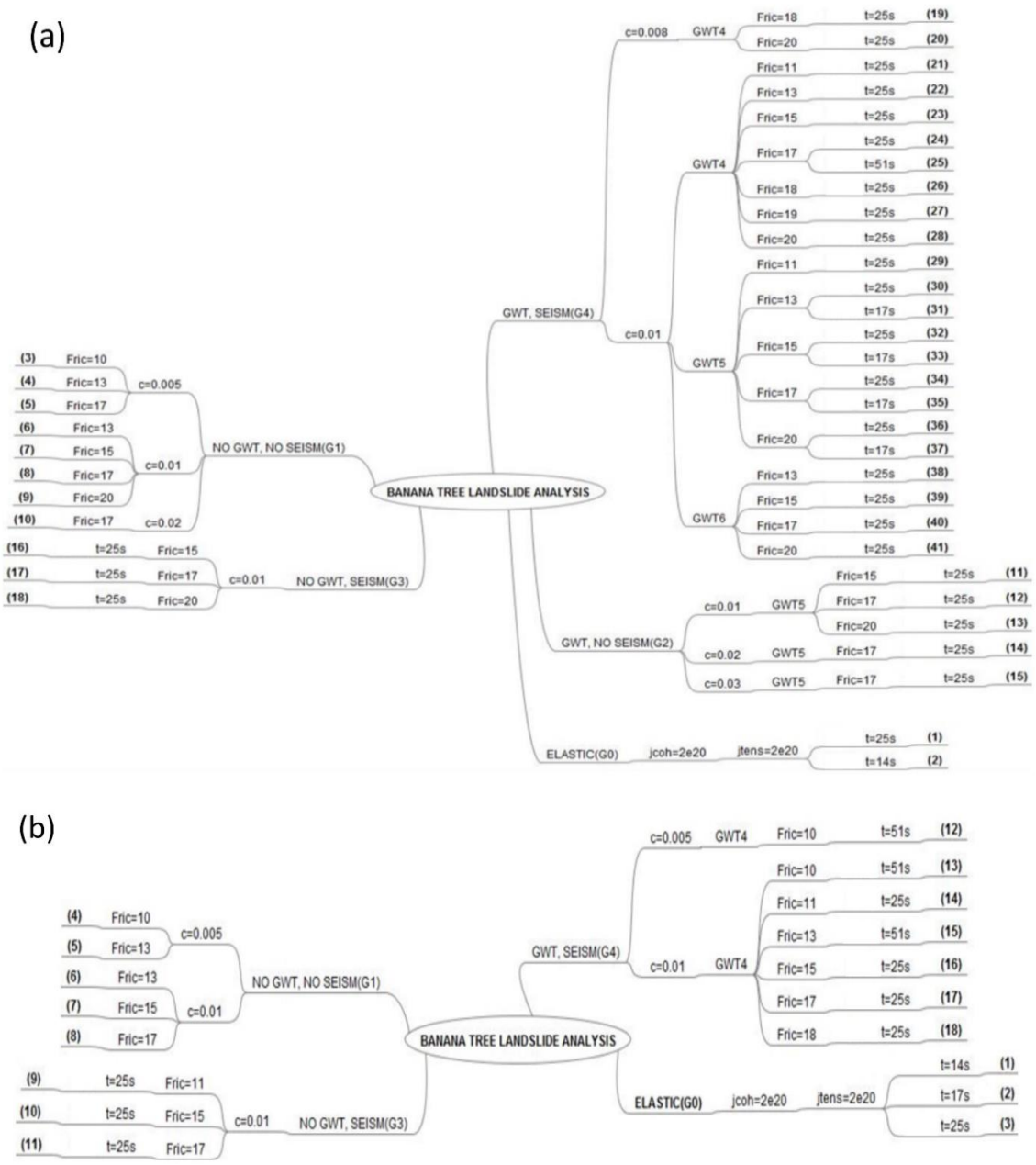

Figure S1. (a) Scenarios for landslide genesis: back analysis (the triggering and evolution up to the actual situation). (b) Landslide stability analysis to simulate possible future evolution. GWT stands for groundwater table, G0 (elastic run made to track the amplification of peak ground acceleration, PGA, and Arias Intensity, Ia, in different parts of the profile), G1 (dry and non-seismic scenarios), G2 (non-seismic and completely or partially saturated scenarios), G3 (dry-seismic scenarios) and G4 (seismic and completely or partially saturated scenarios).

Table S2. Some recent studies of flooding induced by the breaching of landslide dams, and of debris flow routing.

	Model dimensions	Morphodynamics	Flow rheology	Available observations
Present study	2D	No	Turbulent flow	None
Fan et al. (2012)	1D for river flow, 2D for overland flow	No	Turbulent flow	Peak discharge, peak arrival time …
Yang et al. (2013)	Sobek-1D and -2D	No	Turbulent flow	Flooding occurrences
Shrestha and Nakagawa (2016)	1D for river flow	Yes	Granular, hyper-concentrated and turbulent flow	Observed flood discharge
Li et al. (2011)	1D for river flow, 2D sediment transport	Yes	Empirical equations for Mohr-Coulomb, viscous and turbulent shear stresses	Downstream hydrograph, observed sediment depths …
Mergili et al. (2012a)	2D, considering bottom curvature and steep slope effects	Deposition of granular material represented explicitly	Granular flow (Savage-Hutter type model)	Focused on avalanche flows, not flooding due to dam breaching
Mergili et al. (2012b)	2D	Sediment detachment by runoff and routing of debris flow	Semi-deterministic two-parameter friction model	Debris flow travel distance, shape of deposits …

Section S1.

The base flow was estimated using Manning equation:

$$Q = \frac{1}{n} AR^{2/3} S^{1/2} \quad \text{(S1)}$$

with n the Manning roughness coefficient, A the river cross section (m^2), R the hydraulic radius (m) and S the water surface slope ($m\ m^{-1}$). The Manning equation was largely used to estimate the flow discharge in case of lack of direct measurements data (Herschy 2009; Jacobs et al., 2016; Lumbroso and Gaume 2012; Moody and Martin 2001).

The flow was estimated during the rainy season measurements at a 6 m wide cross section downstream the landslide at 20 m in upstream side of the cross section 3 of Fig. 3, with an average water depth of 40 cm. It should be noted that the 6m do not correspond to the full width of the river. The bottom of the river is not flat and the base flow usually follows one or two branches corresponding to the lower part of the minor bed (Fig. 2d). With a local hydraulic slope of 0.01 m m^{-1} and a Manning roughness n of 0.041 $m^{-1/3}s$, Eq. (B1) gives an approximate flow of 2.92 $m^3\ s^{-1}$. A value of 3 $m^3\ s^{-1}$ was used for base flow in the computation scenarios. Manning roughness coefficient was estimated based on channel descriptions given by Barnes (1967).

The steady 20-year and 50-year flows used in the different scenarios were calculated using the rational formula:

$$Q_j = \sum_{k=1}^{j} C_{m,k} i_k A_m \quad \text{(S2)}$$

with i_k the rainfall intensity ($mm\ h^{-1}$), $C_{m,k}$ the runoff coefficient and A_m each of the contributing surfaces (ha); m is defined as equal to $j-k+1$. The constant intensity was derived from the Intensity-Frequency-Duration law of Bujumbura provided by the Geographic Institute of Burundi (IGEBU). Huff (1967) method based was used to approximate the intensity distribution during the project rainfall event. It was developed based on 291 storms analysis and is applicable for catchments up to 1036 km^2 large. The method provides 4 distributions according to the quartile in which the rainfall is heaviest. For the case of Bujumbura, calculations based on the 2nd quartile distribution were judged to approximate better the intensity variation, given that the peak intensity usually occurs in the first 3rd of rainfall duration. Based on Kohler (1951)'s equation on soil saturation index and on the recent work by Mathlouthi and Lebdi (2010) on the Rain-Runoff relationship, there is no doubt that soil saturation during storms can be strongly influenced by other previous rainfall events. In a context of rainy season base flow, the use of variable runoff offers little interest. Hence, a constant runoff coefficient was used. We obtained initial peak flows of 61.6 $m^3\ s^{-1}$ and 123.4 $m^3\ s^{-1}$ for a 20-year and a 50-year flows respectively. Being aware that the use of peak flow corresponds to the extreme scenario, we used 3 $m^3\ s^{-1}$, 60 $m^3\ s^{-1}$ and 120 $m^3\ s^{-1}$ for the base flow, 20-year and 50-year initial discharge. This small decrease can be compensated by the lateral infiltrations as we progress downstream.

Section S2.

To analyse the sensitivity of the results to the downstream boundary condition, we considered the 20 scenarios described in Table S2. We mainly tested two pairs of L and w values:

- in a first configuration (scenarios 1 to 9), the water level at the downstream end of the computational domain depends substantially on the flow rate (L = 35 m, W = 0.185 m);
- in another set of model runs (scenarios 10 to 18), the downstream water level is only weakly influenced by the flow rate (L = 350 ÷ 3500 m, W = 0.185 m).

For each of the two types of downstream boundary conditions, we analysed three different roughness heights and considered three different discharges. Finally, we also tested one configuration in which the downstream water level remains independent of the pre-failure discharge in the river; but still varies under transient flow conditions (scenarios 19 and 20). This was tested only for the intermediate bottom roughness. For the 20 scenarios, three values of discharge were considered: base flow, 20-year flood and 50-year flood. In all the tested scenarios, the influence of the downstream boundary conditions did not extend over a distance exceeding about 300 meters from the downstream end of the computational domain.

Table S3. Considered scenarios for the pre-failure flow conditions.

		Scenario ID	Roughness (m)	Flow ($m^3 s^{-1}$)	L (m)	W (m)
Flow-dependent downstream water level	Relatively smooth bottom	1, 2, 3	0.1	3, 60, 120	35	0.1850
	Intermediate roughness	4, 5, 6	0.2	3, 60, 120	35	0.1850
	Relatively rough bottom	7, 8, 9	0.3	3, 60, 120	35	0.1850
Weakly flow-dependent downstream water level	Relatively smooth bottom	10, 11, 12	0.1	3, 60, 120	350 ÷ 3500	0.2754
	Intermediate roughness	13, 14, 15	0.2	3, 60, 120	350 ÷ 3500	0.2754
	Relatively rough bottom	16, 17, 18	0.3	3, 60, 120	350 ÷ 3500	0.2754
Flow-independent downstream level, except for transients	Intermediate roughness	19	0.2	3	35	1.4088
		20	0.2	60	35	0 .695

Section S3.

Examples of results of Step 1 and Step 2 of the flow modelling procedure are displayed in Fig. S2 and Figs S3 to S6, respectively.

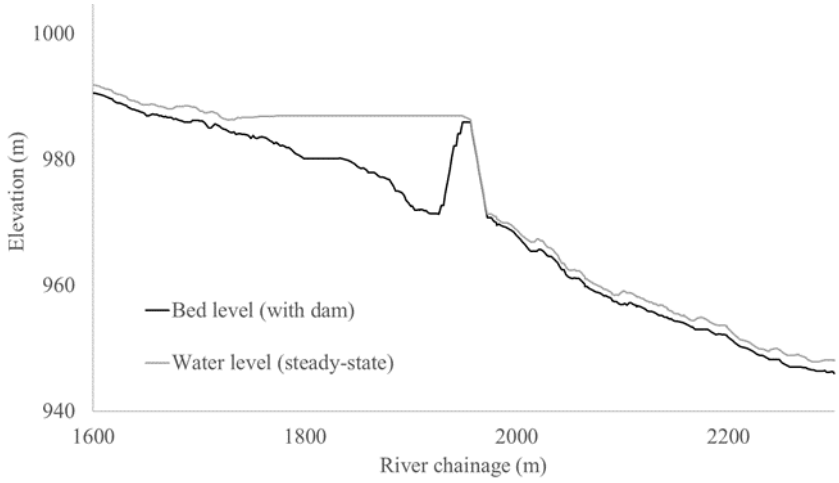

Figure S2. Longitudinal profile (in the dam area) of the bed and water levels for a steady discharge of 120 m³/s, as computed in Step 1 of the hydraulic modelling procedure (k_s = 0.3 m).

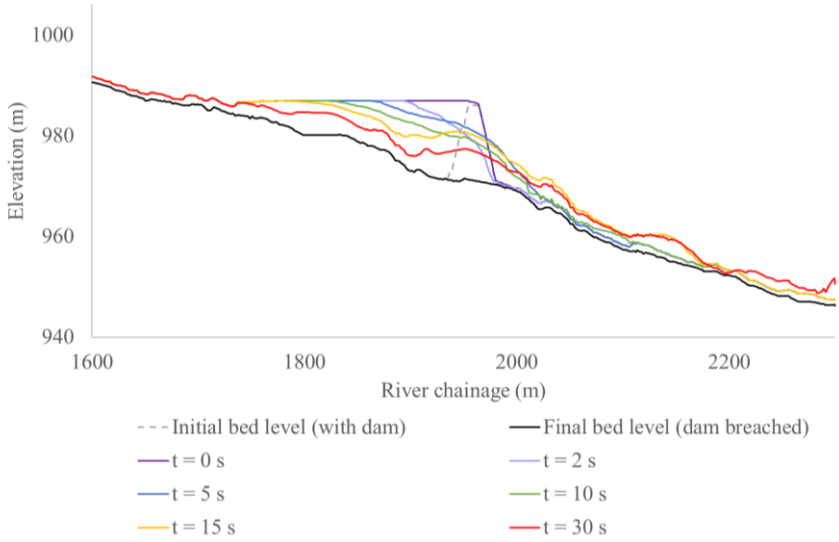

Figure S3. Longitudinal profiles of water levels computed in Step 2 of the hydraulic modelling procedure, assuming an instantaneous breaching of the dam (extreme case) and a flow rate of 120 m³/s in the river prior to dam breaching (k_s = 0.3 m).

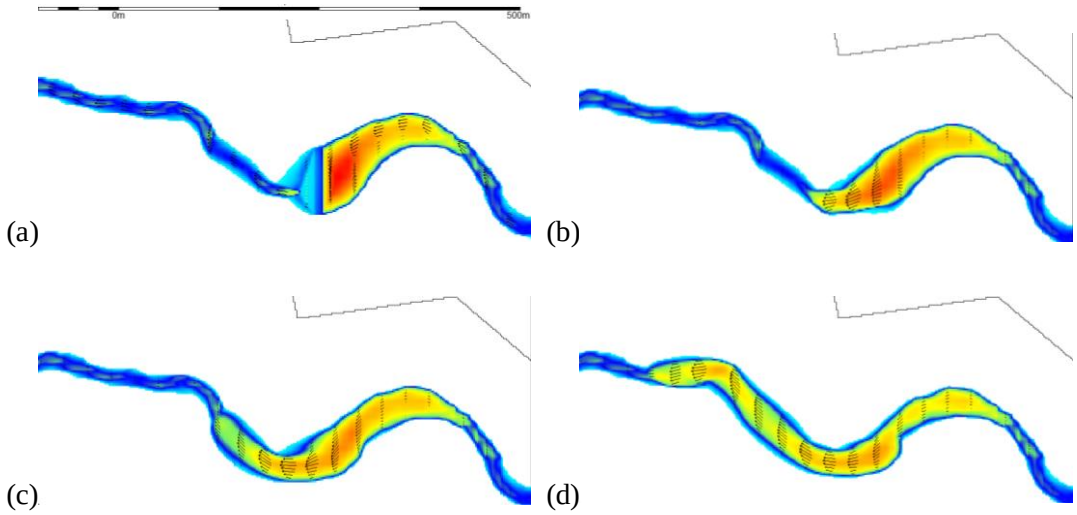

Figure S4. Water depth distribution and velocity profiles before the breaching (a) as well as after 5 s (b), 10 s (c) and 20 s (d), as computed in Step 2 of the hydraulic modelling procedure. This computation assumes an instantaneous breaching of the dam (extreme case) and a flow rate of 120 m³/s in the river prior to dam breaching (k_s = 0.3 m).

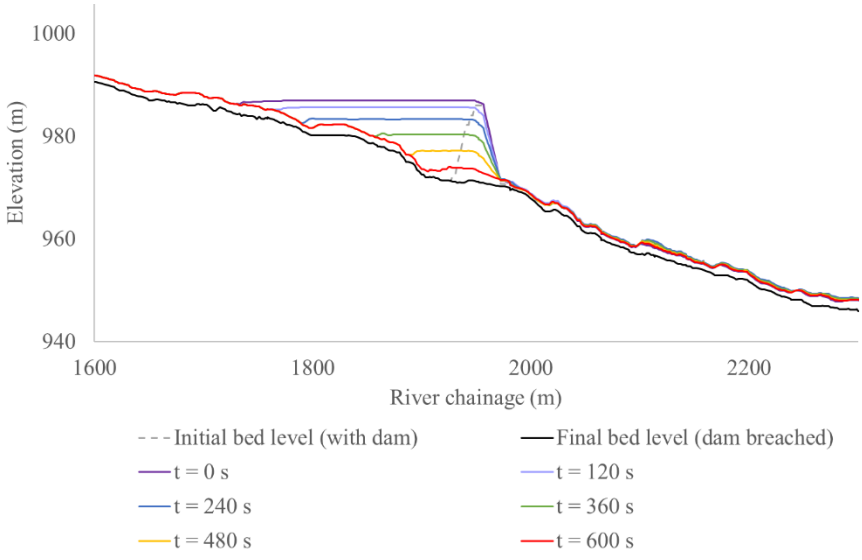

Figure S5. Longitudinal profiles of water levels computed in Step 2 of the hydraulic modelling procedure, assuming a breaching duration of 600 s and a flow rate of 120 m³/s in the river prior to dam breaching (k_s = 0.3 m).

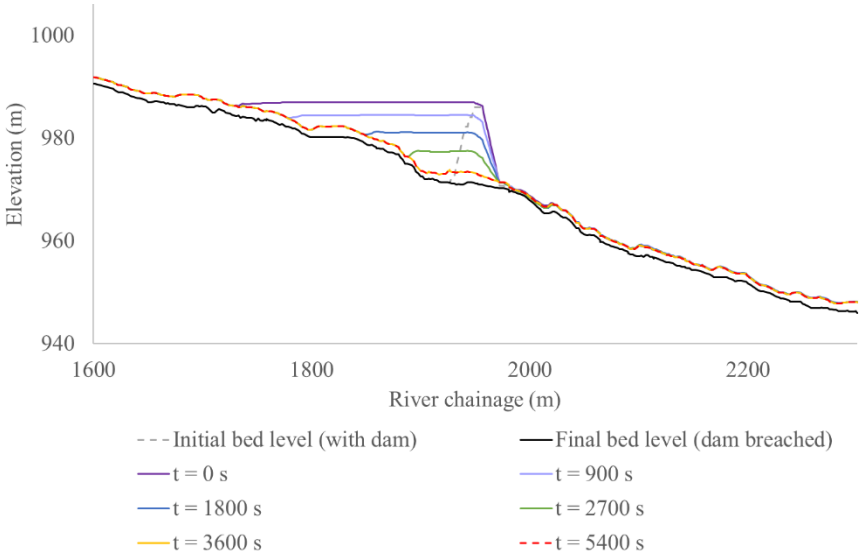

Figure S6. Longitudinal profiles of water levels computed in Step 2 of the hydraulic modelling procedure, assuming a breaching duration of 3600 s and a flow rate of 120 m³/s in the river prior to dam breaching (k_s = 0.3 m).

Table S4. Peak discharge changes (%) at the different cross sections for base flow, 20-year flow and 50-year flow, based on a breaching time of 60 min.

	Changes (%)		
	50-year	20-year	Base flow
Section1	1.25	1.58	4.08
Section2	1.05	1.76	4.18
Section3	0.89	2.05	7.48
Section4	1.09	1.78	5.32

Table S5. Details of the sensibility indicator of floodplain to the topographic data. «I » and «F »stand for « Initial topography » (10 m-resampled) and "Field topography" (corrected by field-measurements); ∩: Intersection, ∪: Union, \: minus. The breaching duration is 60 minutes.

		Count	Area in m^2	Indicator	Average indicator
			k_s = 0.1 m		
Base flow	I\F	12274	49096	0.82	0.83
	F\I	15244	60976		
	I∩F	122610	490440		
	I∪F	150128	600512		
20-year- flow	I\F	10408	41632	0.85	
	F\I	14637	58548		
	I∩F	137162	548648		
	I∪F	162207	648828		
50-year- flow	I\F	17529	70116	0.77	
	F\I	23916	95664		
	I∩F	141801	567204		
	I∪F	183246	732984		
			k_s = 0.3 m		
Base flow	I\F	13361	53444	0.83	
	F\I	11899	47596		
	I∩F	127064	508256		
	I∪F	152324	609296		
20-year- flow	I\F	14583	58332	0.85	
	F\I	10899	43596		
	I∩F	144646	578584		
	I∪F	170128	680512		
50-year- flow	I\F	21693	86772	0.86	
	F\I	9146	36584		
	I∩F	184539	738156		
	I∪F	215378	861512		

References

Barnes, H.: Roughness characteristics of natural channels, U.S. Geological Survey, Water Supply Paper 1849, 1967.

Blair, T.C. and McPherson, J.G.: Grain-size and textural classification of coarse sedimentary particles, Journal of Sedimentary Research, 69, 6–19, 1999.

Fan, X. M., Westen, C. J., Xu, Q., Gorum, T., and Dai, F. C.: Analysis of landslide dams induced by the 2008 Wenchuan earthquake, J. Asian Earth Sci., 57, 25–37, 2012.

Herschy, R.: Streamflow measurement, 3rd edn., Taylor and Francis, New York, 2009.

Huff, F. A.: Time distribution of rainfall in heavy storms, Water Resour. Res., 3, 1007–1019, 1967.

Kohler, M. A. and Linsley, R. K.: Predicting the runoff from storm rainfall, Weather Bureau, US Dept of Commerce, Washington, DC, Research Paper 34, 1951.

Li, M.-H., Sung, R.-T., Dong, J.-J., Lee, C.-T., and Chen, C.-C.: The formation and breaching of a short-lived landslide dam at Hsiaolin Village, Taiwan – Part II: Simulation of debris flow with landslide dam breach, Eng. Geol., 123, 60–71, 2011.

Lumbroso, D. and Gaume, E.: Reducing the uncertainty in indirect estimates of extreme flash flood discharges, J. Hydrol., 414–415, 16–30, https://doi.org/10.1016/j.jhydrol.2011.08.048, 2012.

Mathlouthi, M. and Lebdi, F.: Modélisation de la relation pluie-ruissellement par durée d'épisode pluvieux dans un bassin du nord de la Tunisie, Hydrol. Sci. J., 55, 1111–1122, https://doi.org/10.1080/02626667.2010.512471, 2010.

Mergili, M., Schratz, K., Ostermann, A., and Fellin, W.: Physically-based modelling of granular flows with Open Source GIS, Nat. Hazards Earth Syst. Sci., 12, 187–200, https://doi.org/10.5194/nhess-12-187-2012, 2012a.

Mergili, M., Fellin, W., Moreiras, S. M., and Stötter, J.: Simulation of debris flows in the Central Andes based on Open Source GIS: Possibilities, limitations, and parameter sensitivity, Nat. Hazard, 61, 1051–1081, 2012b.

Moody, J. A. and Martin, D. A.: Post-fire, rainfall intensity-peak discharge relations for three mountainous watersheds in the Western USA, Hydrol. Process., 15, 2981–2993, https://doi.org/10.1002/hyp.386, 2001.

Shrestha, B. and Nakagawa, H.: Hazard assessment of the formation and failure of the Sunkoshi landslide dam in Nepal, Nat. Hazards, 82, 2029–2049, 2016.

Terry, J. P. and Goff, J.: Mega clasts: proposed revised nomenclature at the coarse end of the Udden-Wentworth grain-size scale for sedimentary particles, J. Sediment. Res., 84, 192–197, 2014.

Yang, S. H., Pan, Y. W., Dong, J. J., Yeh, K. C., and Liao, J. J.: A systematic approach for the assessment of flooding hazard and risk associated with a landslide dam, Nat. Hazards, 65, 41–62, 2013.